




## Open Archive Toulouse Archive Ouverte (OATAO)

OATAO is an open access repository that collects the work of Toulouse researchers and makes it freely available over the web where possible

This is an author's version published in: <http://oatao.univ-toulouse.fr/23517>

**Official URL:** <https://doi.org/10.1016/j.electacta.2019.03.080>

**To cite this version:**

Gomes, Maurilio Pereira and Costa, Isolda and Pébère, Nadine  and Rossi, Jesualdo Luiz and Tribollet, Bernard and Vivier, Vincent *On the corrosion mechanism of Mg investigated by electrochemical impedance spectroscopy*. (2019) *Electrochimica Acta*, 306. 61-70. ISSN 0013-4686

Any correspondence concerning this service should be sent to the repository administrator: [tech-oatao@listes-diff.inp-toulouse.fr](mailto:tech-oatao@listes-diff.inp-toulouse.fr)

# On the corrosion mechanism of Mg investigated by electrochemical impedance spectroscopy

Maurilio Pereira Gomes <sup>a, b</sup>, Isolda Costa <sup>b</sup>, Nadine Pébère <sup>c</sup>, Jesualdo Luiz Rossi <sup>b</sup>, Bernard Tribollet <sup>a</sup>, Vincent Vivier <sup>a, \*</sup>

<sup>a</sup> Sorbonne Université, CNRS, Laboratoire Interfaces et Systèmes Electrochimiques, LISE, F-75005, Paris, France

<sup>b</sup> Instituto de Pesquisas Energéticas e Nucleares, Centro de Ciência e Tecnologia de Materiais, Av. Prof. Lineu Prestes, 2242, Cidade Universitária, CEP, 05508-000, São Paulo SP, Brazil

<sup>c</sup> CIRIMAT, Université de Toulouse, CNRS, INPT, UPS, ENSIACET, 4, allée Emile Monso, BP 44362, 31030, Toulouse Cedex 4, France

## A B S T R A C T

This work reported a detailed analysis of the electrochemical impedance spectra obtained for the Mg electrode during immersion in a sodium sulfate solution. A model was proposed which took into account the presence of: (i) a thin oxide film (MgO) which progressively covered the Mg electrode surface, (ii) film-free areas where the Mg dissolution occurs in two consecutive steps, (iii) a thick layer of corrosion products (Mg(OH)<sub>2</sub>), (iv) an adsorbed intermediate (Mg<sup>+</sup><sub>ads</sub>) which is responsible for the chemical reaction allowing the negative difference effect to be explained. From the impedance data analysis, various parameters were extracted such as the thin oxide film thickness, the resistivity at the metal/oxide film interface and at the oxide film/electrolyte interface, the active surface area as a function of the exposure time to the electrolyte, the thickness of the thick Mg(OH)<sub>2</sub> layer and the kinetic constants of the electrochemical reaction.

## Keywords:

Magnesium

Oxide film

Power-law model

Negative difference effect (NDE)

Adsorbed intermediate

## 1. Introduction

The corrosion mechanism of Mg has been the subject of a huge amount of work [1–5], and despite its ubiquity and history, the elementary mechanism remains little understood. This is mainly due to an anomalous phenomenon called the negative difference effect (NDE) which results in an increase of the hydrogen evolution rate when the magnesium is anodically polarized [6,7]. Indeed, even if this phenomenon has been well documented in the literature [4,7–9] and has been observed from various techniques [10–14], the mechanism itself is tricky and the subject has become controversial. At the corrosion potential, there is a good agreement with the global reaction:



and the formation of corrosion products:



The rate of the NDE has been deeply investigated as a function of impurities contained in the Mg [15–18]. Metal impurities (e.g. Fe, Cu, Ni) result in large overpotential for the hydrogen evolution reaction at the Mg corrosion potential. However, from a thermodynamic point of view, even if these impurities act as local cathodes, any shift of the potential towards the anodic domain should result in a decrease of the hydrogen production reaction. Consequently, the metal impurities cannot be the only ones responsible for the NDE, but such behavior has been further investigated for alloying elements [19,20].

Other developments, including film based model [4,21], formation of magnesium hydride [22,23], or formation of univalent Mg [24–26] have been used to make an attempt to explain the NDE. For the latter, the existence of soluble univalent species dissolved in solution remains questionable [4]. Thus, there is still a need to understand how the NDE occurs at the electrode surface. Additionally, the overall corrosion of Mg also leads to the formation of a thin oxide film (in the nanometer range) on the Mg surface in different corrosive environments that has been evidenced using X-ray photoelectron spectroscopy (XPS) [27,28] or time-of-flight

\* Corresponding author.

E-mail address: [vincent.vivier@upmc.fr](mailto:vincent.vivier@upmc.fr) (V. Vivier).

secondary ion mass spectroscopy (ToF SIMS) depth profiles [29,30].

Interestingly, the use of electrochemical impedance spectroscopy (EIS) has already shown to give reliable and reproducible results for the study of Mg corrosion [31–34]. However, the analysis of the impedance spectra was usually limited to the study of the charge transfer resistance and of the polarization resistance [35]. Recently, a mathematical model for describing the inductive loop has been devised in order to account for the production of the excess of hydrogen [36]. This model took into account the evolution of the electrode surface over time, but it was uncorrelated from any kinetic aspect allowing the NDE to be linked to the corrosion mechanism of Mg. Moreover, plotting EIS data in different representations allows further analysis, in particular the determination of the interfacial capacitance [37]. For instance, the use of complex-capacitance representation allows thin oxide layers formed on passivable metals [38–41], or on Mg alloys [42] to be characterized, leading to the evaluation of the oxide layer thickness.

In the present work, a detailed analysis of the corrosion mechanism of Mg in a sodium sulfate solution was undertaken, based on the use of EIS. A particular attention was paid to the interfacial capacitance analysis and to the inductive loop. For the latter, the previous model involving the relaxation of an adsorbed intermediate was further developed [34] and the fitting of the EIS spectra allowed the variation of the kinetic parameters to be obtained as a function of the immersion time in the Na<sub>2</sub>SO<sub>4</sub> solution.

## 2. Experimental

The working electrode consisted in a Mg rod (5 mm in diameter) with a purity of 99.9%; purchased from Goodfellow. The impurity contents of this commercial pure Mg (given by the provider) are (in ppm): Al = 70, Cu = 20, Fe = 280, Mn = 170, Ni < 10, Si = 50 and Zn < 20. The lateral part of the cylinder was insulated with a cathaphoretic paint and in sequence with an epoxy resin thus exposing a disk electrode of 19.6 mm<sup>2</sup> surface area. Before the electrochemical experiments, the electrode was ground with successive SiC abrasive papers up to grit P4000.

All the experiments were performed using a rotating disk electrode (RDE) and a Gamry Ref 600 + potentiostat. The electrode rotation rate was fixed at 1000 rpm. During the experiment, the temperature was maintained at 25 °C and the electrolyte was in contact with air. The experiments were performed in a 0.1 mol L<sup>-1</sup> Na<sub>2</sub>SO<sub>4</sub> electrolytic solution (pro analysis grade) with an initial pH of 5.6. It is generally accepted that SO<sub>4</sub><sup>2-</sup> anions are less aggressive than Cl<sup>-</sup>. Leleu et al. [42] have shown that the corrosion rate of a commercially pure Mg was about four times higher in a NaCl solution than in a Na<sub>2</sub>SO<sub>4</sub> solution. Thus, in the present study a less aggressive electrolyte was chosen to reduce the dissolution of the Mg rod for performing EIS measurements over extended time periods.

The reference and the counter electrodes were a mercury sulfate electrode (MSE) in a saturated potassium sulfate solution ( $E_{\text{MSE}} = 0.64 \text{ V/SHE}$ ) and a platinum gauze of large surface area, respectively.

The anodic and cathodic current/potential curves were plotted separately (two independent measurements) after a preliminary hold time of 2 h at the corrosion potential ( $E_{\text{corr}}$ ). The potential sweep rate was fixed at  $0.167 \text{ mV s}^{-1}$ . The polarization curves were corrected from the ohmic drop, experimentally determined from the high-frequency limit of the impedance diagrams.

Impedance diagrams were obtained under potentiostatic regulation,  $E_{\text{corr}}$ , over a frequency range of 100 kHz to a few mHz with 8 points per decade, using a  $10 \text{ mV}_{\text{rms}}$  sinusoidal voltage. The linearity was checked by varying the amplitude signal. At least two experiments were performed. The obtained impedance diagrams

were always consistent with the Kramers-Kronig relations [43,44].

## 3. Results and discussion

### 3.1. Steady-state measurements

Fig. 1 shows the current/potential curve obtained on the Mg electrode in a  $0.1 \text{ mol L}^{-1}$  Na<sub>2</sub>SO<sub>4</sub> solution after a preliminary 2 h hold time at  $E_{\text{corr}}$ . As previously reported, the anodic polarization curve shows 3 different domains [34]. The first domain, close to the corrosion potential, is almost linear. This behavior might be explained by the formation of a monovalent adsorbed intermediate followed by the formation of the divalent Mg<sup>2+</sup> ion (*vide infra*). The second domain starts at about  $-1.9 \text{ V/MSE}$  for which a significant change in the slope of the curve can be observed. Such behavior could be ascribed to a change of the limiting process in the dissolution mechanism. The last domain, for potentials larger than  $-1.8 \text{ V/MSE}$ , is characterized by a plateau of current of about  $20 \text{ mA cm}^{-2}$ . In the present work, we mainly focused on the study around  $E_{\text{corr}}$ , thus limiting the investigation on the corrosion/dissolution mechanism to the first domain for low dissolution rate.

The cathodic polarization curve corresponds to the hydrogen evolution reaction and shows two different slopes that are difficult to interpret due to the formation of hydrogen bubbles at the electrode surface.

### 3.2. Electrochemical impedance measurements

#### 3.2.1. Impedance diagrams at $E_{\text{corr}}$

Fig. 2a shows the impedance diagrams (Nyquist coordinates) for the Mg electrode obtained at  $E_{\text{corr}}$  as a function of immersion time in the Na<sub>2</sub>SO<sub>4</sub> solution. Independently of the immersion time, the shape of the diagrams is very similar and shows three distinct time constants. In the high-frequency range, the first capacitive loop corresponds to the charge transfer resistance in parallel with the interfacial capacitance. This capacitance will be thoroughly discussed in the following. The medium-frequency time constant is attributed to the diffusion of species inside the porous layer formed by the corrosion products (it has been previously shown that this

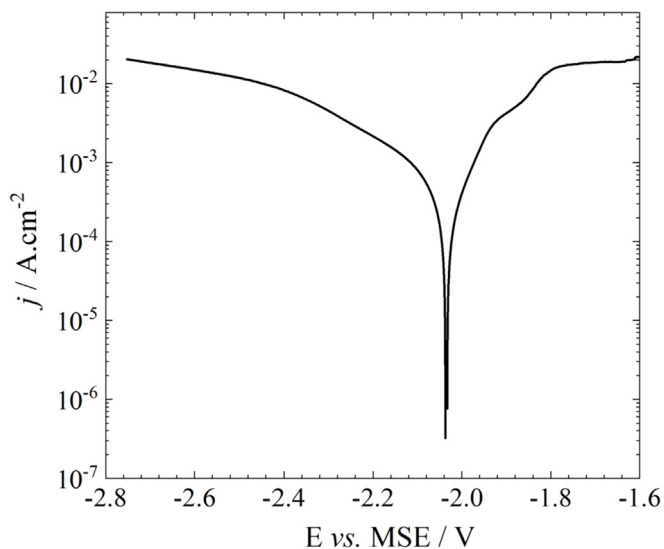


**Fig. 1.** Current/potential curve obtained after 2 h immersion at  $E_{\text{corr}}$  in a  $0.1 \text{ mol L}^{-1}$  Na<sub>2</sub>SO<sub>4</sub> solution ( $\Omega = 1000 \text{ rpm}$ ,  $v = 0.167 \text{ mV s}^{-1}$ ). The anodic and cathodic branches were obtained separately from  $E_{\text{corr}}$  (independent measurements) and the curves were corrected from the ohmic drop.

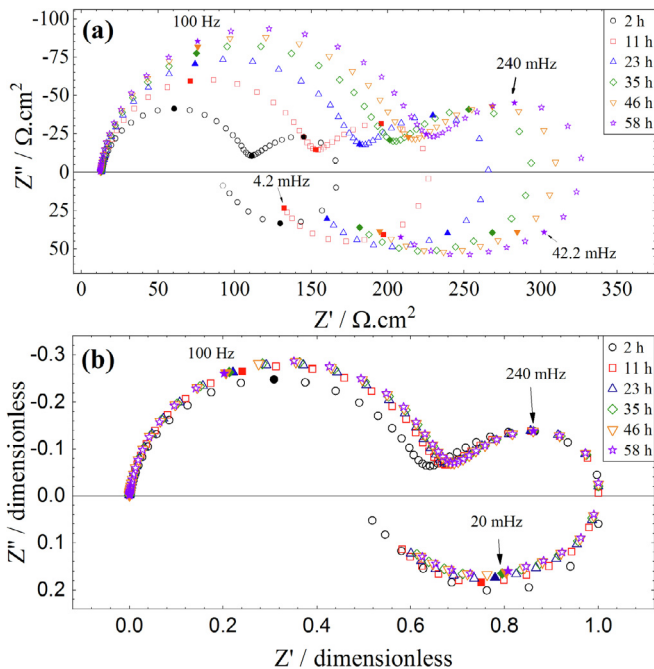


**Fig. 2.** Electrochemical impedance diagrams of Mg after different immersion times at  $E_{\text{corr}}$  in a  $0.1 \text{ mol L}^{-1} \text{ Na}_2\text{SO}_4$  solution ( $\Omega = 1000 \text{ rpm}$ ): (a) raw impedance diagrams (Nyquist representation); (b) normalized impedance diagrams (each diagram was normalized by the maximum value of the real part of the impedance).

time constant was independent of the electrode rotation rate) [32]. The low-frequency inductive loop is ascribed to the relaxation of adsorbed intermediates. Such mechanism, involving a monovalent species adsorbed on the electrode surface, has already been observed for the corrosion of different metals, including Fe [45,46], Cr [47] or Zn [48,49], that is for multi-step reaction mechanism involving adsorbed species [45,50,51].

Interestingly, the impedance diagrams in Fig. 2a are homothetic to each other. This can be better visualized in Fig. 2b (each diagram was normalized by the maximum value of the real part of the impedance). With such a dimensionless representation, all the EIS diagrams superimpose and the three time constants remain unchanged regardless of the immersion time except for the first times (here 2 h). This difference can be ascribed to the reactivity of the bare Mg during the first hours of immersion which will be detailed in a next section. Moreover, the characteristic frequency of the first capacitive loop slightly varies with time. Conversely, the second characteristic frequency corresponding to the diffusion process is constant, in agreement with the RDE theory for the diffusion in a finite-thickness layer. As a result, whatever the frequency domain considered, the variation of the amplitude of the impedance response of each process follows the same proportionality law. This behavior can be attributed to a variation of the active surface area with the immersion time. In other words, the increase of the impedance translates into a decrease in current, that is, in a decrease of the active surface area of the electrode on which the Mg dissolution occurs. It should be noticed that this active surface area is small by comparison with the surface area covered by MgO (see below). This conclusion is in agreement with scanning electrochemical microscopy experiments performed above a corroding Mg substrate that showed a decrease of the surface area of the reactive domain as a function of the immersion time [34].

### 3.2.2. Impedance diagrams at low anodic over potentials: inductive contribution analysis

Fig. 3a shows the impedance diagrams of the Mg electrode after 11 h of immersion in  $0.1 \text{ mol L}^{-1} \text{ Na}_2\text{SO}_4$  solution at  $E_{\text{corr}}$  (black circles) and for two low anodic over potentials (blue squares and red triangles for  $E_{\text{corr}} + 10 \text{ mV}$  and  $E_{\text{corr}} + 20 \text{ mV}$ , respectively). These polarization potentials correspond to steady-state anodic current densities of  $100 \mu\text{A cm}^{-2}$  and  $220 \mu\text{A cm}^{-2}$ , respectively (Fig. 1). It can be seen that the global shape of the two impedance diagrams is independent of the applied potential and shows the same time constants as those previously described, indicating that the same mechanism occurs at  $E_{\text{corr}}$  and for low anodic over potentials. Fig. 3b shows the dimensionless representation of the EIS diagrams obtained from the normalization by the maximum value of the real part of each spectrum presented in Fig. 3a. It can be seen that each time constant slightly depends on the potential. In particular, the amplitude of the low-frequency inductive loop increases with the potential, regardless of the variation of the active surface area. Such observation has been already reported for this inductive feature, but only to evaluate the Mg dissolution rate [35]. Indeed, this inductive contribution can be ascribed to an adsorbed intermediate relaxation and fulfill the hypothesis of the surface coverage relaxation with the potential. In the present case, within the small anodic investigated potential domain, the  $\text{Mg}_{\text{ads}}^+$  surface coverage increases with the potential. Also, it should be mentioned that the existence of adsorbed intermediates has been proposed for many different systems, regardless of the technique used, impedance spectroscopy or polarization curves [52–54].

The intermediate frequency domain corresponding to the diffusion of species through the  $\text{Mg}(\text{OH})_2$  layer is slightly affected by the change in potential.

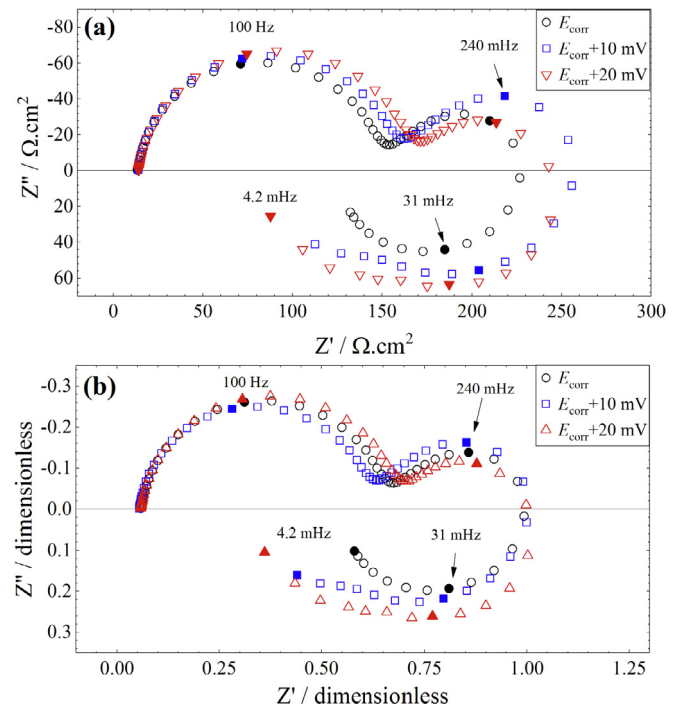


**Fig. 3.** Electrochemical impedance diagrams of Mg in a  $0.1 \text{ mol L}^{-1} \text{ Na}_2\text{SO}_4$  solution ( $\Omega = 1000 \text{ rpm}$ ) at  $E_{\text{corr}}$  and for two anodic over potentials: (a) raw impedance diagrams (Nyquist representation); (b) normalized impedance diagrams (each diagram was normalized by the maximum value of the real part of the impedance).

### 3.2.3. Interfacial capacitance: graphical analysis and power-law model

The impedance results, presented in Fig. 2 and in Fig. 3, show that the high-frequency response corresponding to the charge transfer resistance in parallel with the interfacial capacitance is characterized by a flattened capacitive loop. Graphical analysis of the results allows a constant phase element (CPE) to be clearly evidenced in the high-frequency domain (Fig. 4a) and the  $\alpha$  parameter of the CPE (the impedance of which is given by  $Z_{CPE} = \frac{1}{Q(j\omega)^\alpha}$ ) to be determined from the variation of the imaginary part of the impedance (in absolute value) as a function of frequency (Fig. 4b) [37,55]. In Fig. 4a, it can be seen that the phase angle value on the plateau, for the corrected curve, is  $-79^\circ$ . Thus, the CPE parameter is equal to  $79:90 = 0.88$ , in agreement with the value determined in Fig. 4b. The plateau observed at high-frequency is characteristic of a pure CPE behavior which may be the consequence of a resistivity distribution along the thin oxide film thickness. This CPE behavior can be analyzed by the power-law model [56,57]. However, the use of the power-law model introduces a large number of parameters. The capacitance of the oxide film can

be extracted from the impedance data by using the complex-capacitance representation [58,59] and then, the oxide film thickness can be calculated. It was shown that this methodology allows an easy determination of the oxide film thickness that agrees well with the results obtained with other techniques, such as XPS [38] or reflectometry [41]. A similar methodology has been recently used to investigate the stability of the oxides film formed on a Mg alloy containing rare-earth elements [42]. Thus, in a first step, the film capacitance was graphically determined from the EIS response through the relationship:

$$C(\omega) = \frac{1}{j\omega[Z_F(\omega) - R_e]} \quad (3)$$

Where  $Z_F$  is the impedance of the Mg electrode and  $R_e$  is the electrolyte resistance, which can be determined from the high frequency limit of the impedance diagram.

The results presented in Fig. 5 shows an example of the complex-capacitance plot obtained from the impedance response of the Mg electrode after 35 h of immersion at  $E_{corr}$  in  $0.1 \text{ mol L}^{-1}$   $\text{Na}_2\text{SO}_4$  solution (Fig. 2). From the HF frequency limit of the impedance,  $C_\infty$ , the dielectric capacitance of the thin MgO oxide film formed at the electrode surface can be determined. The thin oxide film thickness,  $\delta_{ox}$ , was afterwards calculated from the usual relationship

$$C_\infty = \frac{\epsilon\epsilon_0}{\delta_{ox}} \quad (4)$$

where  $\epsilon$  and  $\epsilon_0$  are the relative permittivity of the thin oxide film and the vacuum permittivity ( $\epsilon_0 = 8.8510^{-14} \text{ Fcm}^{-1}$ ), respectively. Assuming a permittivity value of 9 for MgO, this leads to an oxide film thickness of 6.6 nm for the results presented in Fig. 5. The oxide film thickness was calculated from all the impedance spectra obtained at  $E_{corr}$ . The  $\delta_{ox}$  values are reported in Fig. 6 as a function of the immersion time in the  $\text{Na}_2\text{SO}_4$  solution. The film thickness slightly increases with time from 5.4 nm up to 7 nm after 60 h of immersion.

Then, the power-law model, previously introduced to account

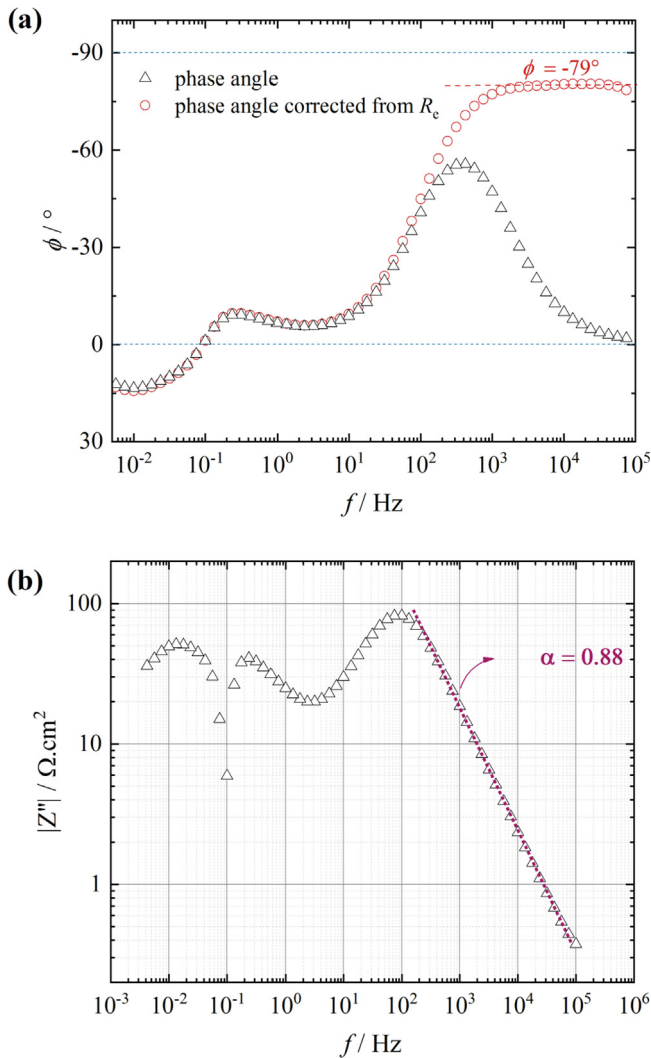


**Fig. 4.** Electrochemical impedance response of Mg after 35 h immersion at  $E_{corr}$  in a  $0.1 \text{ mol L}^{-1}$   $\text{Na}_2\text{SO}_4$  solution ( $\Omega = 1000 \text{ rpm}$ ). (a) Variations of the phase angle (circle) and corrected phase angle from the ohmic resistance (triangle) as a function of the frequency; (b) variations of the absolute value of the imaginary part of the impedance as a function of the frequency.

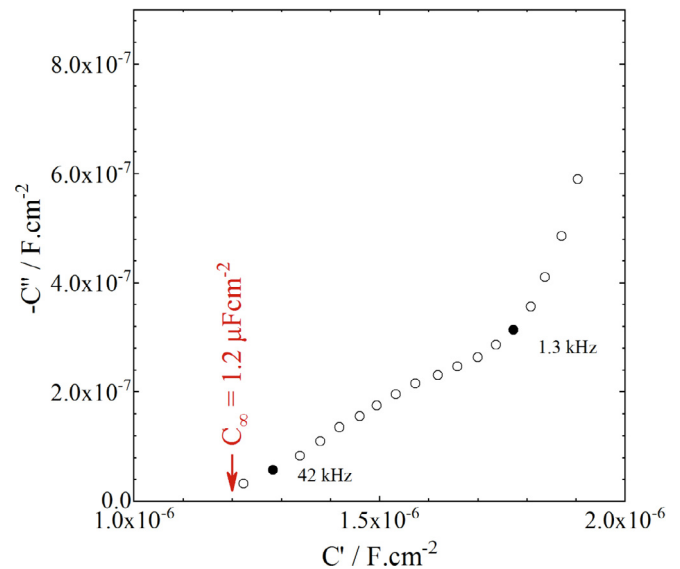


**Fig. 5.** Complex-capacitance plot obtained from the electrochemical impedance response of Mg after 35 h immersion in a  $0.1 \text{ mol L}^{-1}$   $\text{Na}_2\text{SO}_4$  solution ( $\Omega = 1000 \text{ rpm}$ ) – from the data presented in Fig. 4 using Eq. (3). The axis is not orthonormal to make the extrapolation to the  $C'$  axis better visible.



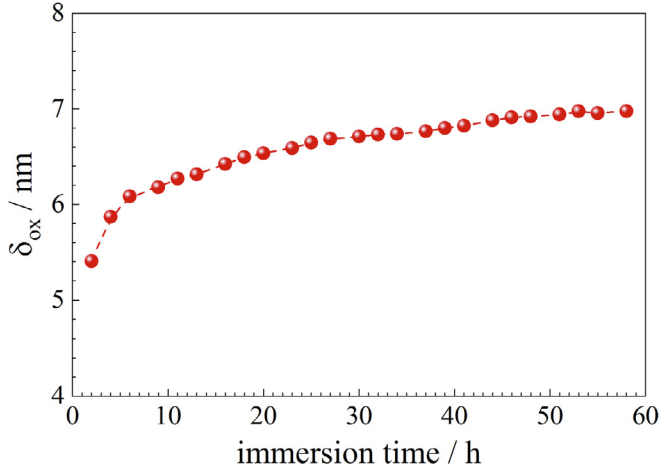


**Fig. 6.** Oxide film thickness formed on the Mg surface as a function of the immersion time in a  $0.1 \text{ molL}^{-1} \text{ Na}_2\text{SO}_4$  solution ( $\Omega = 1000 \text{ rpm}$ ) – Each point of this curve corresponds to the analysis of the complex-capacitance plot as shown in Fig. 5.

for a normal distribution of the time constants at an interface [56,57], was used for describing the impedance contribution of the oxide film and is given by the general formula

$$Z_{\text{oxide}}(\omega) = \int_0^{\delta_{\text{ox}}} \frac{\rho(x)}{1 + j\omega\epsilon\epsilon_0\rho(x)} dx \quad (5)$$

in which  $\omega$  is the pulsation,  $j$  the imaginary number solution of  $j^2 = -1$ , and  $\rho(x)$  the resistivity distribution inside the film, which is expressed as a function of the normal coordinate,  $x$ , to the film as

$$\rho(x) = \rho_{\delta} \left[ \frac{\rho_{\delta}}{\rho_0} + \left( 1 - \frac{\rho_{\delta}}{\rho_0} \right) \left( \frac{x}{\delta_{\text{ox}}} \right)^{\gamma} \right]^{-1} \quad (6)$$

where  $\rho_0$  and  $\rho_{\delta}$  are the boundary values of the resistivity at the metal/oxide interface and at the oxide/solution interface, respectively.

It has been previously shown that this impedance has an analytical solution in a restricted frequency domain depending on the value of  $\rho_0$  and  $\rho_{\delta}$  [56,57]. In the present work, the non-linear regression analysis was performed with the integral formula, which is valid over the whole frequency domain.

The parameters,  $\rho_0$  and  $\rho_{\delta}$ , corresponding to the interfacial capacitances were determined and are reported as a function of the immersion time in Fig. 7. Both at the metal/oxide interface and at the oxide/solution interface the resistivity values remain relatively constant. These values show that the MgO conductivity changes by about 6 orders of magnitude over a nanometric distance. This should be explained by the hydration of the layer that should decrease along the thin film thickness. These constant values are also in agreement with the fact that the oxide film (MgO) mainly grows laterally over the electrode surface decreasing the active surface area as it can be observed on the variation of the impedance diagrams with the immersion time.

Finally, it can be assumed that the thin MgO oxide film dominates the capacitive response of the interface, that is, the surface area covered by the MgO is higher in comparison with the film-free area and thus, the double layer capacitance is negligible.

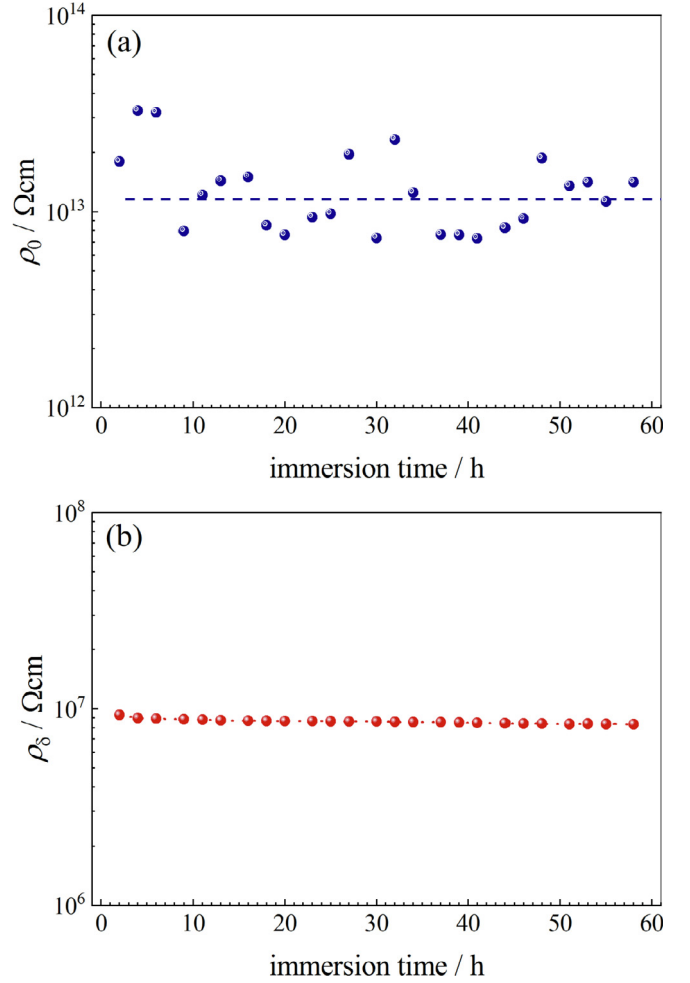


**Fig. 7.** (a) Resistivity at the metal/oxide interface and (b) at the oxide/solution interface of the MgO thin film as a function of the immersion time for the corrosion of Mg in a  $0.1 \text{ molL}^{-1} \text{ Na}_2\text{SO}_4$  solution ( $\Omega = 1000 \text{ rpm}$ ). These data were obtained from the fitting procedure assuming a power-law model for the description of the interfacial capacitance (see text).

### 3.3. Corrosion mechanism

#### 3.3.1. Kinetics model

From the above results, a detailed description of the impedance response can be provided accounting for both, the corrosion mechanism of the Mg in sulfate solution and the interfacial capacitance of the electrode. Unlike most of the literature, we provide a mechanistic description of the corrosion mechanism in terms of elementary reactions together with the analysis of the CPE behavior accounting for the thin oxide film at the Mg surface. Such an approach allows to avoid the use of electrical equivalent circuits, and allows to demonstrate the significant role played by the adsorbates on the corrosion mechanism.

At  $E_{\text{corr}}$ , the description of the corrosion mechanism of a metal accounts for both the anodic and the cathodic processes, resulting in a null net current. In the case of Mg, the impedance results (Figs. 2 and 3) showed that, at  $E_{\text{corr}}$  and for low anodic potential values, the impedance diagrams shows the same time constants, the impedances only increased by a multiplying factor depending on the immersion time. Thus, it can be concluded that the Mg dissolution dominates the impedance response and in the following, only the anodic reaction was taken into account to describe the dissolution mechanism of Mg that is valid at  $E_{\text{corr}}$  and

for low anodic over potentials. Moreover, the anodic steady-state curve and the inductive loop observed on all the EIS diagrams suggest that the mechanism involved an adsorbed intermediate. Hence, it is proposed a corrosion mechanism involving the  $Mg_{ads}^+$  species that remains as an active site on the electrode surface. Interestingly, such an intermediate has been previously proposed by Baril et al. [34] and is also in agreement with the recent works of Taylor [60] and Yuwono et al. [15] involving the formation of adsorbed intermediates at the electrode surface leading to the formation of hydrogen bubbles.

Thus, on the film-free areas, two successive anodic reactions occur



and

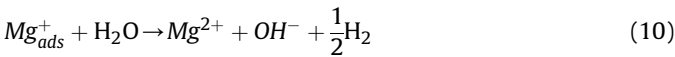


where  $k_i$  and  $k_{-i}$  are the forward and the backward rate constants of the reaction, respectively and expressed in  $cm^{-2} s^{-1}$ . Assuming that the kinetic constants of the electrochemical reactions follow the Tafel's law, each reaction has a normalized time constant  $K_i$  corresponding to its rate constant  $k_i$  by

$$K_i = k_i \exp \left[ \pm b_i (E - E^0) \right] \quad (9)$$

where  $b_i$  is the charge transfer coefficient, and  $(E - E^0)$  the applied over potential with respect to the origin of potentials,  $E^0$ . The sign in the exponential term is positive for an oxidation reaction and negative for a reduction reaction. In the following, the origin of potentials is chosen as the corrosion potential obtained after reaching the steady-state in solution, and thus  $V = E - E_{corr}$ .

For the NDE, which is a chemical reaction of the  $Mg_{ads}^+$ , formed on the Mg surface, with water to produce dihydrogen (Eq. (10)) the increase of the magnitude of the inductive loop, observed on the EIS diagrams as a function of the applied potential (Fig. 3), indicated that the surface coverage by the adsorbed species also increased with the potential. Such a behavior is in agreement with the relaxation of adsorbed species [37,61] and also with the increase of the  $H_2$  formation when the potential of the Mg electrode is shifted towards anodic values. It is thus proposed that the NDE occurs only with the  $Mg_{ads}^+$ , and expresses as



Assuming that the adsorbate  $Mg_{ads}^+$  obeys a Langmuir's isotherm with a maximum number of sites per surface unit  $\beta$ , and a fraction of surface coverage  $\theta$ , the charge and mass balance express as

$$\beta \frac{d\theta}{dt} = K_1(1 - \theta) - K_2\beta\theta + K_{-2}C_{Mg^{2+}} - k_3\beta\theta \quad (11)$$

$$D \frac{C_{Mg^{2+}}}{\delta_{corr}} = K_2\beta\theta - K_{-2}C_{Mg^{2+}} + k_3\beta\theta \quad (12)$$

where  $C_{Mg^{2+}}$  is the interfacial concentration of  $Mg^{2+}$  in solution.  $\delta_{corr}$  is the total thickness of the corrosion product layer. It should be recalled that  $\delta_{corr}$  accounts for the thickness of the  $Mg(OH)_2$  and is different from the MgO film thickness ( $\delta_{ox}$ ), previously determined from the capacitance plots (Fig. 5). The faradaic current expresses as

$$i_F = FA \left[ K_1(1 - \theta) + K_2\beta\theta - K_{-2}C_{Mg^{2+}} \right] \quad (13)$$

where  $F$  is the Faraday constant and  $A$  is the electrode surface area.

At steady-state,  $\frac{d\theta}{dt} = 0$ , which leads to the determination of steady-state  $Mg^{2+}$  concentration and surface coverage as

$$\theta_{stat} = \frac{K_1 + K_{-2}C_{Mg^{2+}}}{K_1 + K_2\beta + k_3\beta} \quad (14)$$

and

$$C_{Mg^{2+}} = \frac{(K_2 + k_3)\beta\theta_{stat}}{\frac{D}{\delta_{corr}} + K_{-2}} \quad (15)$$

thus

$$\theta_{stat} = \frac{K_1 \left( \frac{D}{\delta_{corr}} + K_{-2} \right)}{K_1 \left( \frac{D}{\delta_{corr}} + K_{-2} \right) + (K_2 + k_3)\beta \frac{D}{\delta_{corr}}} \quad (16)$$

The linearization of the governing equations allows the calculation of the faradaic impedance as the solution of the linear system of equations Eqs. (17)–(19):

$$j\omega\beta\Delta\theta = -(K_1 + K_2\beta + k_3\beta)\Delta\theta + (K_1b_1 - K_1b_1\theta - K_2b_2\beta\theta - K_{-2}b_{-2}C_{Mg^{2+}})\Delta V + K_{-2}\Delta C_{Mg^{2+}} \quad (17)$$

$$(j\omega\beta + K_1 + \beta(K_2 + k_3))\Delta\theta = (K_1b_1(1 - \theta) - K_2b_2\beta\theta - K_{-2}b_{-2}C_{Mg^{2+}})\Delta V + K_{-2}\Delta C_{Mg^{2+}} \quad (18)$$

$$\frac{\Delta i_F}{FA} = (K_2\beta - K_1)\Delta\theta + (K_1b_1 - K_1b_1\theta_1 + K_2b_2\beta\theta + K_{-2}b_{-2}C_{Mg^{2+}})\Delta V - K_{-2}\Delta C_{Mg^{2+}} \quad (19)$$

The concentration variation  $\Delta C_{Mg^{2+}}$  inside a finite diffusion layer of thickness  $\delta_{corr}$  is given by the solution of the second Fick's law using the Nernst hypothesis [37].

$$\frac{\Delta C_{Mg^{2+}}}{\Delta i_F} = -\frac{1}{FAD} \frac{\tanh\left(\delta_{corr}\sqrt{\frac{j\omega}{D}}\right)}{\sqrt{\frac{j\omega}{D}}} = -\frac{1}{FA}N(\omega) \quad (20)$$

with

$$N(\omega) = \frac{\tanh\left(\delta_{corr}\sqrt{\frac{j\omega}{D}}\right)}{\sqrt{j\omega D}} \quad (21)$$

then, the faradaic contribution to the impedance can be calculated

$$Z_F(\omega) = \frac{\Delta V}{\Delta i_F} = \frac{1 + K_{22}N(\omega) \left[ 1 - \frac{(K_2\beta - K_1)}{(j\omega\beta + K_1 + \beta(K_2 + k_3))} \right]}{FA \left[ (r_1 + r_2) + \frac{(K_2\beta - K_1)(r_1 - r_2)}{(j\omega\beta + K_1 + \beta(K_2 + k_3))} \right]} \quad (22)$$

with

$$r_1 = K_1 b_1 (1 - \theta) \quad (23)$$

and

$$r_2 = K_2 b_2 \beta \theta + K_{22} b_{22} C_{Mg^{2+}} \quad (24)$$

The overall impedance is then obtained by taking into account the contribution of the interfacial capacitance,  $Z_{oxide}(\omega)$ , and the electrolyte resistance,  $R_e$ :

$$Z(\omega) = R_e + \frac{Z_F(\omega) \times Z_{oxide}(\omega)}{Z_F(\omega) + Z_{oxide}(\omega)} \quad (25)$$

Fig. 8 shows the EIS diagram in Nyquist representation for the Mg electrode after 35 h immersion (black circles). On the same graph, the result of the non-linear regression with the proposed model (Eqs. (22) and (25)) is reported (red crosses). This non-linear regression was performed with an in-house made software based on a simplex algorithm allowing analytical expression of the impedance and of the conductivity to be used. A detailed analysis of the EIS diagrams presented in Figs. 2 and 3 was performed with the model, and in the following, the results of this analysis and the variations of the most significant parameters are presented and discussed. The electrolyte resistance remains constant as a function of the immersion time. Such behavior is expected since  $R_e$  is measured in the high-frequency domain and only depends on the geometry of the electrochemical cell, and in particular of the electrode size. Thus, for the fitting procedure, the  $R_e$  value was graphically determined and then used as a constant. Similarly, the thin oxide film thicknesses ( $\delta_{ox}$ ) determined from the complex-capacitance diagrams (Fig. 6) were also fixed in the fitting procedure. Thus, the number of parameters to be adjusted was smaller allowing a greater accuracy for the remaining parameters to be obtained. It should also be underline that this model enables to explain both the dissolution kinetics of Mg with a two-elementary-step reaction mechanism and the NDE phenomenon, is in agreement with the experimental results of the literature [2–6].

### 3.3.2. Modeling of the electrochemical response

From the fitting procedure, the thickness of the  $Mg(OH)_2$  layer formed on the electrode surface during the corrosion process can be readily obtained. Its variation as a function of the immersion

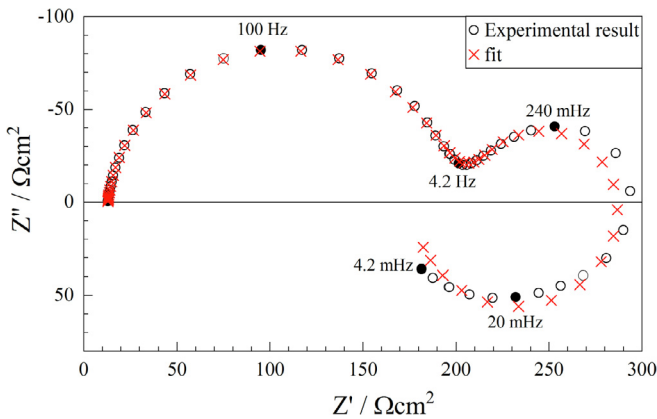


**Fig. 8.** Impedance response of Mg after 35 h immersion in a 0.1 molL<sup>-1</sup> Na<sub>2</sub>SO<sub>4</sub> solution ( $\Omega = 1000$  rpm) in a Nyquist representation (black circles) and fitting of the EIS response with the model (Eqs. (22) and (25)) (red crosses). The fitted diagram corresponds to the following parameters:  $b_1 = 28.9 \text{ V}^{-1}$ ,  $b_2 = 11.8 \text{ V}^{-1}$ ,  $b_{-2} = 9.3 \text{ V}^{-1}$ ,  $k_1 = 2.3210^{-10} \text{ cm}^2 \text{ s}^{-1}$ ,  $k_2 = 9.3510^{-2} \text{ cm}^2 \text{ s}^{-1}$ ,  $k_{-2} = 7.5810^{-4} \text{ cm}^2 \text{ s}^{-1}$ ,  $k_3 = 8.1610^{-3} \text{ cm}^2 \text{ s}^{-1}$ ,  $\delta_{corr} = 22.2 \mu\text{m}$ ,  $\delta_{ox} = 6.7 \text{ nm}$ ,  $D = 3 \cdot 10^{-6} \text{ cm}^2 \text{ s}^{-1}$ ,  $\beta = 10^{-6} \text{ mol cm}^{-2}$ .

time in the Na<sub>2</sub>SO<sub>4</sub> solution is presented in Fig. 9. It slightly decreases from 29  $\mu\text{m}$  to 21  $\mu\text{m}$  after about 60 h of immersion. A thickness, in the same order of magnitude (15  $\mu\text{m}$ ), has been measured from *ex situ* SEM examination of the cross-section of the  $Mg(OH)_2$  layer formed at a Mg sample after 21 h of immersion in a sodium sulfate solution [32]. Most of the variation of the layer thickness is observed during the first hours of immersion. Indeed, no corrosion product was initially present, and the thickness variation in the first hours is a result of two phenomena: the convective diffusion of redox species in solution for short immersion time (*i.e.* during the formation of the corrosion layer, the thickness of the Nernst layer being in the range of 20  $\mu\text{m}$  for a RDE at 1000 rpm), and then the diffusion inside the corrosion layer for longer immersion time. After 20 h, it is assumed that a steady-state is reached between the formation and the dissolution of the  $Mg(OH)_2$  layer. A general sketch of the interface is presented in Fig. 10.

The calculation of the surface coverage by the adsorbate  $Mg_{ads}^{+}$  with Eq. (16) and the regressed parameters showed a variation of  $\theta_{stat}$  that increased during the 10 first hours from  $2 \times 10^{-3}$  to  $4 \times 10^{-3}$ , and then decreased down to  $3 \times 10^{-3}$ , in agreement with the progressive formation of the corrosion products layer that partially hindered the surface reactivity. Moreover, from Eq. (15), the interfacial concentration of  $Mg^{2+}$  was calculated. Values in the range of a few  $10^{-7} \text{ mol L}^{-1}$  were obtained, that is 2–3 orders of magnitude lower than the solubility limit of  $Mg(OH)_2$  for a pH of about 10 [31,32]. Such a value is in agreement with a local pH increase at the Mg surface and the presence of a concentration gradient in the close vicinity of the electrode.

In contrast, the variation of the different kinetic constants, which were obtained from the fitting of the different time constants, cannot be directly interpreted. Indeed, the evolution of the EIS diagrams as a function of the immersion time strongly depends on the variation of the active surface area, and thus the fitted parameters, obtained from the raw data, must be corrected from the surface area variation. The evolution of the active surface area was calculated from the charge transfer resistance, determined from the diameter of the first capacitive loop of the impedance diagram for each immersion time and by using the first measurement (after 2 h of immersion) as reference value. The results are presented in Fig. 11. It should be noted that the same result is obtained if the active surface area is calculated from the maximum value of the real part of the impedance diagrams as it was done for performing the normalization of the EIS spectra presented in Fig. 2. A significant

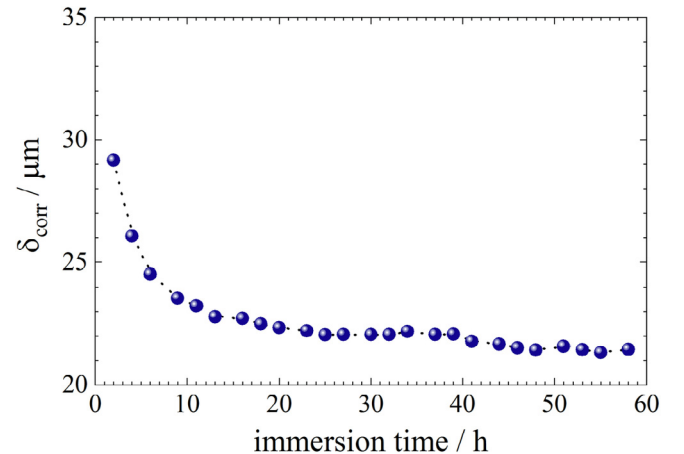


**Fig. 9.** Total thickness of the corrosion layer formed on Mg surface as a function of the immersion time in a 0.1 molL<sup>-1</sup> Na<sub>2</sub>SO<sub>4</sub> solution ( $\Omega = 1000$  rpm) – obtained from the fitting of the impedance diagram as exemplified in Fig. 8.



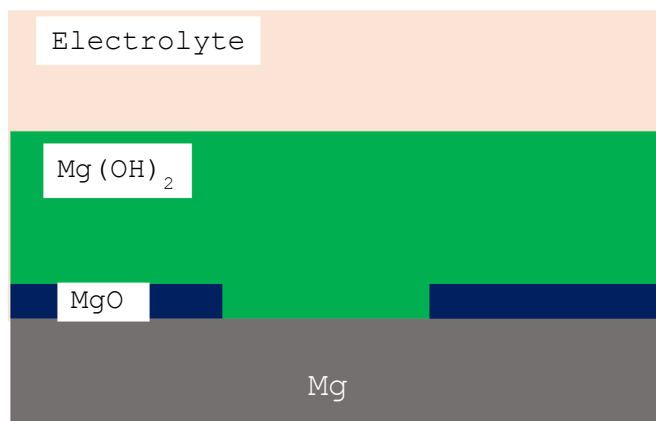


**Fig. 10.** Sketch of the interface describing the different layers formed during the Mg corrosion. According to the impedance data analysis, the MgO layer thickness is about 5–7 nm (Fig. 7) and the Mg(OH)<sub>2</sub> layer thickness is about 20–30 μm (Fig. 9).

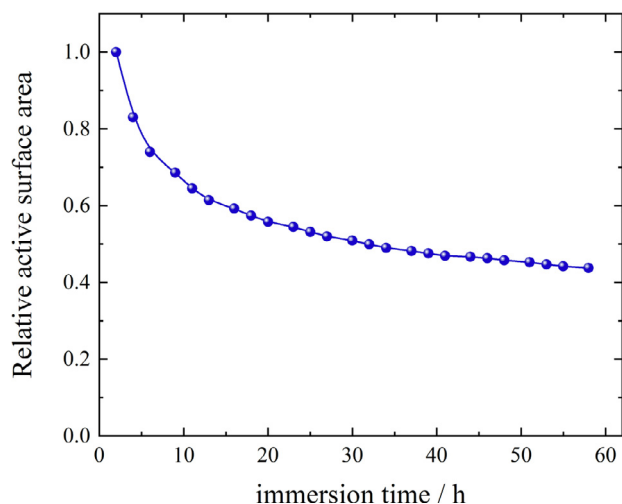


**Fig. 11.** Active surface area as a function of the immersion time for Mg in a 0.1 mol·L<sup>-1</sup> Na<sub>2</sub>SO<sub>4</sub> solution (Ω = 1000 rpm). The relative surface area was calculated from the charge transfer resistance, determined from the diameter of the first capacitive loop of the impedance diagram for each immersion time (Fig. 2) and by using the first measurement performed after 2 h of immersion as reference value.

decrease of the active surface with time can be observed (in other words, an increase of the electrode surface area covered by the oxide layer), which is about twice smaller after 60 h of immersion. Even if the active surface area cannot be accurately determined and should represent a small fraction of the whole electrode surface, the obtained variation underlines that the oxide film does not completely cover the electrode surface (free-film area still remains present on the Mg surface). This is in agreement with the Pilling-Bedworth (PB) ratio. For pure MgO, the PB ratio is smaller than 1 (0.8 [5,62]) indicating that the MgO oxide film cannot fully cover the Mg surface.

The fitting procedure allows all the parameters of the model to be determined. The variations of the kinetic constants,  $k_1$  and  $k_2$ , and the related Tafel parameters,  $b_1$  and  $b_2$ , are presented in Fig. 12 as a function of time. The variation of the raw values of  $k_1$  (open blue circles - Fig. 12a) shows a decrease of the kinetic constant with time. However, the active surface area also varies as a function of time (Fig. 11) and the apparent kinetics parameters obtained from the impedance variations can be described as extensive parameters. The variations of  $k_1$  have to be corrected from the active

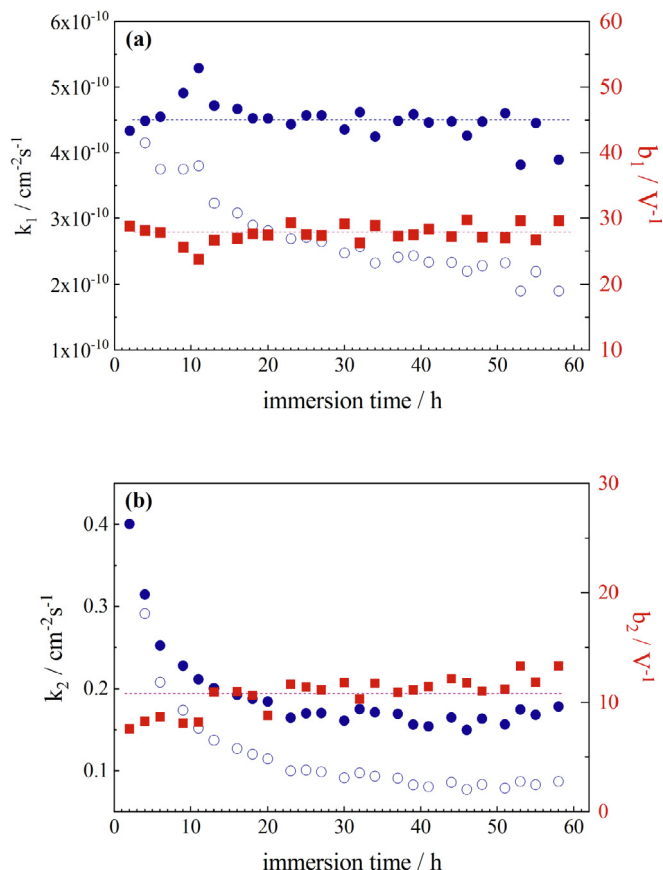


**Fig. 12.** Kinetic parameters as a function of the immersion time for the corrosion of Mg in a 0.1 mol·L<sup>-1</sup> Na<sub>2</sub>SO<sub>4</sub> solution (Ω = 1000 rpm) – the blue open circles correspond to the raw kinetic constant determined from the fitting procedure; the blue plain circles are the same data corrected from the surface variations (see text); the red squares correspond to the variation of the Tafel coefficient.

surface area variations (plain blue circles - Fig. 12a), thus showing an almost constant behavior with time. The Tafel's coefficient,  $b_1$  (red squares - Fig. 12a) is independent of the immersion time. It should be noted that this parameter, the units of which are V<sup>-1</sup>, is to be seen as an intensive parameter, i.e. independent of the surface variation. It is thus concluded that the first step of the anodic dissolution is not modified by the formation of the corrosion product or by the minute change of the interface. Conversely, the second kinetic constant  $k_2$  (Fig. 12b) varies whatever the representation, whereas  $b_2$  remains constant. Thus, the second step (dissolution rate of Mg, from adsorbed species,  $\text{Mg}_{\text{ads}}^+$ , to  $\text{Mg}^{2+}$ ) is governed by the immersion time. These kinetic parameters allowed the steady-state current to be calculated, using Eq. (13), which corresponds in this case to the corrosion current density. After 2 h of immersion, the value is about 115 μA cm<sup>-2</sup>, which is in agreement with the current densities measured on the current/potential curve (Fig. 2). This value is close to that obtained in similar conditions (commercially pure Mg in Na<sub>2</sub>SO<sub>4</sub> solution with a RDE) [63].

It can be concluded that the impedance measurements which allowed the evaluation of the corrosion rate from the charge transfer resistance, showed that the variation of the active surface area of the Mg electrode is mainly responsible for the apparent decrease of the corrosion rate as a function of time.

#### 4. Conclusions

In the present work, a model was proposed to fully describe the

three time constants observed on the impedance diagrams as a function of the immersion time in a sodium sulfate solution. The Mg dissolution was described by an elementary mechanism involving the exchange of two electrons in two steps and including an adsorbed intermediate ( $Mg_{ads}^{+}$ ). The  $Mg_{ads}^{+}$  is involved in a chemical reaction to describe the NDE (Eq. (10)). All the impedance diagrams were perfectly adjusted with the model.

First, the increase of the impedance magnitude with time was ascribed to the decrease of the active surface area. In the high-frequency range, the charge transfer resistance in parallel with the interfacial capacitance allows a fine description of the thin oxide MgO film formed on the Mg surface. Its thickness was obtained from the analysis of the complex capacitance plot, whereas the CPE behavior was explained and analyzed by using the power-law model that describes the resistivity variations inside the film [56,57].

The second time constant was attributed to the diffusion of electroactive species inside the thick-layer of corrosion products ( $Mg(OH)_2$ ), as previously described in the literature [34].

Finally, the inductive loop in the low-frequency domain was ascribed to the relaxation of the adsorbate on the Mg surface. It was shown that its magnitude increased with the anodic over potentials, showing that the adsorbed intermediates can be specific sites on which the NDE occurs.

## Acknowledgments

The authors acknowledge FAPESP (2013/13235-6) and CAPES-Cofecub (806-14) for the financial support to this research and also for the grant of Maurilio Pereira Gomes (88881.154406/2017-01).

## References

- [1] G. Song, A. Atrons, Corrosion mechanisms of magnesium alloys, *Adv. Eng. Mater.* 1 (1999) 11–33.
- [2] G. Song, A. Atrons, Understanding magnesium corrosion: a framework for improved alloy performance, *Adv. Eng. Mater.* 5 (2003) 837–858.
- [3] A. Atrons, G. Song, M. Liu, Z. Shi, F. Cao, M.S. Dargusch, Review of recent developments in the field of magnesium corrosion, *Adv. Eng. Mater.* 17 (2015) 400–453.
- [4] S. Thomas, N.V. Medhekar, G.S. Frankel, N. Biribilis, Corrosion mechanism and hydrogen evolution on Mg, *Curr. Opin. Solid State Mater. Sci.* 19 (2015) 85–94.
- [5] M. Esmaily, J.E. Svensson, S. Fajardo, N. Biribilis, G.S. Frankel, S. Virtanen, R. Arrabal, S. Thomas, L.G. Johansson, Fundamentals and advances in magnesium alloy corrosion, *Prog. Mater. Sci.* 89 (2017) 92–193.
- [6] G.L. Makar, J. Kruger, Corrosion of magnesium, *Int. Mater. Rev.* 38 (1993) 138–153.
- [7] G.S. Frankel, S. Fajardo, B.M. Lynch, Introductory lecture on corrosion chemistry: a focus on anodic hydrogen evolution on Al and Mg, *Faraday Discuss* 180 (2015) 11–33.
- [8] G.S. Frankel, A. Samaniego, N. Biribilis, Evolution of hydrogen at dissolving magnesium surfaces, *Corros. Sci.* 70 (2013) 104–111.
- [9] S. Fajardo, G.S. Frankel, A kinetic model explaining the enhanced rates of hydrogen evolution on anodically polarized magnesium in aqueous environments, *Electrochem. Commun.* 84 (2017) 36–39.
- [10] G. Williams, N. Biribilis, H.N. McMurray, The source of hydrogen evolved from a magnesium anode, *Electrochem. Commun.* 36 (2013) 1–5.
- [11] G. Song, A. Atrons, Recent insights into the mechanisms of magnesium corrosion and research suggestions, *Adv. Eng. Mater.* 9 (2007) 177–183.
- [12] S. Fajardo, G.S. Frankel, Gravimetric method for hydrogen evolution measurements on dissolving magnesium, *J. Electrochem. Soc.* 162 (2015) C693–C701.
- [13] J. Swiatowska, P. Volovitch, K. Ogle, The anodic dissolution of Mg in NaCl and Na<sub>2</sub>SO<sub>4</sub> electrolytes by atomic emission spectroelectrochemistry, *Corros. Sci.* 52 (2010) 2372–2378.
- [14] V. Shkirskiy, A.D. King, O. Gharbi, P. Volovitch, J.R. Scully, K. Ogle, N. Biribilis, Revisiting the electrochemical impedance spectroscopy of magnesium with online inductively coupled plasma atomic emission spectroscopy, *Chem-PhysChem* 16 (2015) 536–539.
- [15] J.A. Yuwono, N. Biribilis, R. Liu, Q. Ou, Q. Bao, N.V. Medhekar, Aqueous electrochemical activity of the Mg surface: the role of group 14 and 15 microalloying elements, *J. Electrochem. Soc.* 164 (2017) C918–C929.
- [16] S. Fajardo, O. Gharbi, N. Biribilis, G.S. Frankel, Investigating the effect of ferrous ions on the anomalous hydrogen evolution on magnesium in acidic ferrous chloride solution, *J. Electrochem. Soc.* 165 (2018) C916–C925.
- [17] O. Gharbi, N. Biribilis, Clarifying the dissolution mechanisms and electrochemistry of Mg<sub>2</sub>Si as a function of solution pH, *J. Electrochem. Soc.* 165 (2018) C497–C501.
- [18] S. Fajardo, G.S. Frankel, Effect of impurities on the enhanced catalytic activity for hydrogen evolution in high purity magnesium, *Electrochim. Acta* 165 (2015) 255–267.
- [19] A. Samaniego, N. Biribilis, X. Xia, G.S. Frankel, Hydrogen evolution during anodic polarization of Mg alloyed with Li, Ca, or Fe, *Corrosion* 71 (2014) 224–233.
- [20] S. Fajardo, J. Bosch, G.S. Frankel, Anomalous hydrogen evolution on AZ31, AZ61 and AZ91 magnesium alloys in unbuffered sodium chloride solution, *Corros. Sci.* 146 (2019) 163–171.
- [21] J.L. Robinson, P.F. King, Electrochemical behavior of the magnesium anode, *J. Electrochem. Soc.* 108 (1961) 36–41.
- [22] G.G. Perrault, Potentiostatic study of the magnesium electrode in aqueous solution, *J. Electroanal. Chem.* 27 (1970) 47–58.
- [23] E. Gulbrandsen, J. Taftø, A. Olsen, The passive behaviour of Mg in alkaline fluoride solutions. Electrochemical and electron microscopical investigations, *Corros. Sci.* 34 (1993) 1423–1440.
- [24] Z.M. Shi, J.X. Jia, A. Atrons, Galvanostatic anodic polarisation curves and galvanic corrosion of high purity Mg in 3.5% NaCl saturated with Mg(OH)<sub>2</sub>, *Corros. Sci.* 60 (2012) 296–308.
- [25] Z.M. Shi, F.Y. Cao, G.L. Song, A. Atrons, Low apparent valence of Mg during corrosion, *Corros. Sci.* 88 (2014) 434–443.
- [26] A.D. Atrons, I. Gentile, A. Atrons, Possible dissolution pathways participating in the Mg corrosion reaction, *Corros. Sci.* 92 (2015) 173–181.
- [27] H.B. Yao, Y. Li, A.T.S. Wee, An XPS investigation of the oxidation/corrosion of melt-spun Mg, *Appl. Surf. Sci.* 158 (2000) 112–119.
- [28] M. Santamaria, F. Di Quarto, S. Zanna, P. Marcus, Initial surface film on magnesium metal: a characterization by X-ray photoelectron spectroscopy (XPS) and photocurrent spectroscopy (PCS), *Electrochim. Acta* 53 (2007) 1314–1324.
- [29] A. Seyeux, M. Liu, P. Schmutz, G. Song, A. Atrons, P. Marcus, ToF-SIMS depth profile of the surface film on pure magnesium formed by immersion in pure water and the identification of magnesium hydride, *Corros. Sci.* 51 (2009) 1883–1886.
- [30] D. Mercier, J. Świątowska, S. Zanna, A. Seyeux, P. Marcus, Role of segregated iron at grain boundaries on Mg corrosion, *J. Electrochem. Soc.* 165 (2018) C42–C49.
- [31] N. Pebere, C. Riera, F. Dabosi, Investigation of magnesium corrosion in aerated sodium sulfate solution by electrochemical impedance spectroscopy, *Electrochim. Acta* 35 (1990) 555–561.
- [32] G. Baril, N. Pebere, The corrosion of pure magnesium in aerated and deaerated sodium sulfate solutions, *Corros. Sci.* 43 (2001) 471–484.
- [33] G. Baril, C. Blanc, M. Keddam, N. Pebere, Local electrochemical impedance spectroscopy applied to the corrosion behavior of an AZ91 magnesium alloy, *J. Electrochem. Soc.* 150 (2003) B488–B493.
- [34] G. Baril, G. Galicia, C. Deslouis, N. Pebere, B. Tribollet, V. Vivier, An impedance investigation of the mechanism of pure magnesium corrosion in sodium sulfate solutions, *J. Electrochem. Soc.* 154 (2007) C108–C113.
- [35] A.D. King, N. Biribilis, J.R. Scully, Accurate electrochemical measurement of magnesium corrosion rates; a combined impedance, mass-loss and hydrogen collection study, *Electrochim. Acta* 121 (2014) 394–406.
- [36] M. Curioni, L. Salamone, F. Scenini, M. Santamaria, M. Di Natale, A mathematical description accounting for the superfluous hydrogen evolution and the inductive behaviour observed during electrochemical measurements on magnesium, *Electrochim. Acta* 274 (2018) 343–352.
- [37] M.E. Orazem, B. Tribollet, *Electrochemical Impedance Spectroscopy*, 2 ed., Wiley, Hoboken, New Jersey, 2017.
- [38] M. Benoit, C. Bataillon, B. Gwinner, F. Miserque, M.E. Orazem, C.M. Sánchez-Sánchez, B. Tribollet, V. Vivier, Comparison of different methods for measuring the passive film thickness on metals, *Electrochim. Acta* 201 (2016) 340–347.
- [39] T.T.M. Tran, B. Tribollet, E.M.M. Sutter, New insights into the cathodic dissolution of aluminium using electrochemical methods, *Electrochim. Acta* 216 (2016) 58–67.
- [40] S. Chakri, I. Frateur, M.E. Orazem, E.M.M. Sutter, T.T.M. Tran, B. Tribollet, V. Vivier, Improved EIS analysis of the electrochemical behaviour of carbon steel in alkaline solution, *Electrochim. Acta* 246 (2017) 924–930.
- [41] S. Chakri, A.N. Patel, I. Frateur, F. Kanoufi, E.M.M. Sutter, T.T.M. Tran, B. Tribollet, V. Vivier, Imaging of a thin oxide film formation from the combination of surface reflectivity and electrochemical methods, *Anal. Chem.* 89 (2017) 5303–5310.
- [42] S. Leleu, B. Rives, J. Bour, N. Causse, N. Pèbère, On the stability of the oxides film formed on a magnesium alloy containing rare-earth elements, *Electrochim. Acta* 290 (2018) 586–594.
- [43] C. Gabrielli, M. Keddam, H. Takenouti, Kramers-Kronig Transformation in Relation to the Interface Regulating Device, vol. 1188, ASTM Special Technical Publication, STP, 1993, pp. 140–153.
- [44] J.R. Macdonald, Some new directions in impedance spectroscopy data analysis, *Electrochim. Acta* 38 (1993) 1883–1890.
- [45] I. Epelboin, C. Gabrielli, M. Keddam, H. Takenouti, Model of the anodic behavior of iron in sulfuric acid medium, *Electrochim. Acta* 20 (1975) 913–916.
- [46] I. Epelboin, M. Keddam, O.R. Mattos, H. Takenouti, The dissolution and

- passivation of iron and iron-chromium alloys in acidified sulfate medium. Influences of pH and chromium content, *Corros. Sci.* 19 (1979) 1105–1112.
- [47] J.A.L. Dobbelaar, J.H.W. de Wit, Impedance measurements and analysis of the corrosion of chromium, *J. Electrochem. Soc.* 137 (1990) 2038–2046.
- [48] C. Cachet, F. Ganne, G. Maurin, J. Petitjean, V. Vivier, R. Wiart, EIS investigation of zinc dissolution in aerated sulfate medium. Part I: bulk zinc, *Electrochim. Acta* 47 (2001) 509–518.
- [49] C. Cachet, F. Ganne, S. Joiret, G. Maurin, J. Petitjean, V. Vivier, R. Wiart, EIS investigation of zinc dissolution in aerated sulphate medium. Part II: zinc coatings, *Electrochim. Acta* 47 (2002) 3409–3422.
- [50] I. Epelboin, M. Keddam, J.C. Lestrade, Faradaic impedances and intermediates in electrochemical reactions, *Faraday Discuss. Chem. Soc.* 56 (1973) 264–275.
- [51] D. Klotz, Negative capacitance or inductive loop? – a general assessment of a common low frequency impedance feature, *Electrochem. Commun.* 98 (2019) 58–62.
- [52] J.O.M. Bockris, D. Drazic, A.R. Despic, The electrode kinetics of the deposition and dissolution of iron, *Electrochim. Acta* 4 (1961) 325–361.
- [53] K.E. Heusler, R. Knödler, Die kinetik der zinkelektrode in wässrigen malonatlösungen, *Electrochim. Acta* 18 (1973) 855–861.
- [54] W.J. Lorenz, J.R. Vilche, Zur kinetik der anodischen eisenauflösung im neutralen medium, *Corros. Sci.* 12 (1972) 785–798.
- [55] M.E. Orazem, N. Pebere, B. Tribollet, Enhanced graphical representation of electrochemical impedance data, *J. Electrochem. Soc.* 153 (2006) B129–B136.
- [56] B. Hirschorn, M.E. Orazem, B. Tribollet, V. Vivier, I. Frateur, M. Musiani, Constant-phase-element behavior caused by resistivity distributions in films: II. Applications, *J. Electrochem. Soc.* 157 (2010) C458–C463.
- [57] B. Hirschorn, M.E. Orazem, B. Tribollet, V. Vivier, I. Frateur, M. Musiani, Constant-phase-element behavior caused by resistivity distributions in films: I. Theory, *J. Electrochem. Soc.* 157 (2010) C452–C457.
- [58] A.K. Jonscher, Dielectric characterisation of semiconductors, *Solid State Electron.* 33 (1990) 737–742.
- [59] A.K. Jonscher, Dielectric relaxation in solids, *J. Phys. D Appl. Phys.* 32 (1999) R57–R70.
- [60] C.D. Taylor, A first-principles surface reaction kinetic model for hydrogen evolution under cathodic and anodic conditions on magnesium, *J. Electrochem. Soc.* 163 (2016) C602–C608.
- [61] R. Antaño-López, M. Keddam, M. Turmine, V. Vivier, The impedance response of a passive film revisited by a double modulation technique, *ChemElectroChem* 6 (2019) 202–210.
- [62] F. Cao, G.-L. Song, A. Atrens, Corrosion and passivation of magnesium alloys, *Corros. Sci.* 111 (2016) 835–845.
- [63] S. Leleu, B. Rives, N. Causse, N. Pébère, Corrosion rate determination of rare-earth Mg alloys in a Na<sub>2</sub>SO<sub>4</sub> solution by electrochemical measurements and inductive coupled plasma-optical emission spectroscopy, *Journal of Magnesium and Alloys* (2019). <https://doi.org/10.1016/j.jma.2018.12.002>.